Kinetic Modeling of the Effect of MAO/Zr Ratio and Chain Transfer to Aluminum in Zirconocene Catalyzed Propylene Polymerization

Bernabe Quevedo-Sanchez,‡ Jessica F. Nimmons,‡ E. Bryan Coughlin,*,† and Michael A. Henson*,‡

Department of Chemical Engineering and Department of Polymer Science and Engineering, University of Massachusetts, Amherst, Massachusetts 01003

Received April 19, 2006; Revised Manuscript Received April 28, 2006

ABSTRACT: A kinetic model based on the coordination−insertion mechanism was developed to characterize metallocene-catalyzed propylene polymerization using two different catalyst systems: *rac*-Et(Ind)$_2$ZrCl$_2$/MAO (**I**/MAO) and *rac*-Et(4,7-Me$_2$-1-Ind)$_2$ZrCl$_2$/MAO (**II**/MAO). Slurry propylene polymerizations were performed in a semibatch reactor at 40 °C to investigate the effects of propylene partial pressure and MAO/Zr ratio. The kinetic model accounts for the formation of regioirregularities, the occurrence of chain transfer to trimethylaluminum (TMA), and β-hydride chain transfer to both monomer and metal to predict the effects of propylene partial pressure and the MAO concentration on polymer molecular weight and the formation of isobutyl end groups. A systematic optimization strategy was applied to estimate the kinetic parameters from on-line measurements of the reaction rate and end-of-batch measurements of the molecular weights and percentages of end groups. The formation of 2,1-insertions was more frequent for catalyst **II**/MAO (k_s = 97.4 L mol^{-1} s^{-1} vs k_s = 49.4 L mol^{-1} s^{-1} for **I**/MAO). The M_w of polymer produced with **I**/MAO decreased at low pressures due to the high rate of monomolecular β-hydride transfer to the metal (k_H = 26.5 s^{-1}). Chain transfer to TMA was more significant with the catalyst **II**/MAO ($k_{Al} = 5.46 \times 10^{+3}$ L mol^{-1} s^{-1} vs $k_{Al} = 1.97 \times 10^{+3}$ L mol^{-1} s^{-1} for **I**/MAO).

Introduction

The ability to control regio- and stereochemistry, and comonomer content and distribution are some of the important advantages that metallocene catalysts afford in the polymerization of olefins. The development of new catalyst structures and the control over reaction conditions allow the production of polyolefins with tailored properties.[1−5] Accurate modeling of the coordination/insertion polymerization of olefins with metallocene catalysts is essential to understanding the effect of process conditions on polymer properties.[6−11] In the slurry polymerization of olefins using homogeneous metallocene catalysts, the most important reaction conditions are temperature, pressure and cocatalyst content.

The most commonly used cocatalyst for the metallocene-catalyzed production of polyolefins is methylaluminoxane (MAO).[12,13] The formation of an alkylated activated complex from metallocene molecules and MAO results from an equilibrium reaction. Thus, increasing amounts of MAO will produce a higher concentration of activated complex, thereby increasing polymerization activity.[14,15] The amount of MAO used at an industrial scale is restricted by its high cost, which represents an economic disadvantage compared to Ziegler−Natta catalysts. Residual trimethylaluminum (TMA) present in the MAO solution acts as a chain transfer agent, which decreases the polymer molecular weight if chain transfer to TMA becomes competitive with propagation. Thus, the concentration of MAO affects both the polymerization rate and the molecular weight of the polymer produced.

The effect of chain transfer to trialkylaluminum compounds on molecular weight of isotactic polypropylene (iPP) depends on the catalyst system and reaction conditions.[15−18] For the benchmark catalyst system *rac*-ethylenebis(indenyl)zirconium dichloride/MAO (**I**/MAO), significant chain transfer to aluminum was detected when AlEt$_3$ combined with Ph$_3$CB(C$_6$F$_5$)$_4$ was used as cocatalyst.[17] The conditions at which the addition of free TMA may have a significant effect on the molecular weight of i-PP, catalyzed by **I**/MAO, are yet to be explored. Generally, the selectivity of chain transfer to aluminum is enhanced at low polymerization temperatures[17−19] and at low propylene concentrations.[15,20] Polypropylene with only aluminum-terminated chains has been produced with the highly isospecific catalyst *rac*-Me$_2$Si(2-Me-4-Naph-Ind)$_2$ZrCl$_2$/MAO at 10 °C and 1 bar of propylene pressure.[19] Aluminum-terminated chains of iPP have the potential to be valuable precursors for chain-end functionalized polypropylenes[21] and polypropylene block copolymers.[22]

Kinetic models have been developed to characterize homogeneous polymerization of ethylene and propylene using metallocene catalyst systems.[6−10,23,24] Few models include chain transfer reactions to predict the molecular weight distribution of polymer chains.[6,7,23,24] Ochoteco et al.[10] modeled the effect of Al/Zr ratio on reaction rate, assuming the formation of more active species with increasing MAO concentration. Their kinetic model successfully predicted the reaction rate at different Al/Zr ratios for the slurry polymerization of propylene catalyzed by Cp$_2$ZrCl$_2$ at 40 °C. The kinetic model developed by Huang et al.[7] was the first, and only, attempt to include the effect of chain transfer to aluminum on molecular weight. They estimated kinetic parameters from average values of polymerization rate and active complex concentration, reporting a transfer rate constant to aluminum equal to 1 L mol^{-1} s^{-1} at 40 °C for the Et(H$_4$Ind)$_2$ZrCl$_2$/MAO complex.

In our previous work, we developed a kinetic model for **I**/MAO to predict the effect of temperature and propylene partial pressure on reaction rate, molecular weight distribution (MWD) and percentages of vinylidene and butenyl end groups.[25] In this study, we have extended the applicability of the model to include the effect of MAO/Zr molar ratio on reaction rate, MWD and

* To whom correspondence should be addressed. E-mail: (E.B.C.) coughlin@mail.pse.umass.edu; (M.A.H.) henson@ecs.umass.edu.
† Department of Polymer Science and Engineering, University of Massachusetts.
‡ Department of Chemical Engineering, University of Massachusetts.

10.1021/ma060880n CCC: $33.50
Published on Web 06/01/2006

Table 1. Polymerization Conditions and Activity for Runs with I/MAO

run[a]	*T* (°C)	*P* (atm)	MAO/Zr (mol/mol)	TMA/Zr[b] (mol/mol)	Zr (μmol)	[M][c] (mol/L)	activity (kgPP/(mol Zr[M] h))
1	40	1.0	3000	464	10.0	0.44	5101
2	40	1.5	3000	464	8.0	0.69	5954
3	40	2.5	3000	464	4.0	1.19	8631
4	40	2.5	6000	928	4.0	1.19	8558
5	40	2.5	10 000	1543	4.0	1.19	10 228
6	40	2.5	18 000	2777	4.0	1.19	10 972
7	40	3.5	3000	464	3.0	1.71	11 541
8	40	4.0	3000	464	2.0	1.97	23 000

[a] Polymerization conditions: Catalyst **I**/MAO; 200 mL of toluene; agitation speed 1250 rpm. [b] TMA is a residual component in MAO solution. [c] Propylene concentration in toluene was calculated using the Peng−Robinson equation of state for vapor and liquid phases in equilibrium.

Table 2. Polymerization Conditions and Activity for Runs with II/MAO

run[a]	*T* (°C)	*P* (atm)	MAO/Zr (mol/mol)	TMA/Zr[b] (mol/mol)	Zr (μmol)	[M][c] (mol/L)	activity (kgPP/(mol Zr[M] h))
9	40	1.5	1000	154	5.0	0.69	7567
10	40	2.5	1000	154	5.0	1.19	5898
11	40	2.5	8000	1234	5.0	1.19	11 003
12	40	2.5	15 000	2315	5.0	1.19	14 548
13	40	3.5	1000	154	5.0	1.71	7479

[a] Polymerization conditions: Catalyst **I**/MAO; 200 mL of toluene; agitation speed 1250 rpm. [b] TMA is a residual component in MAO solution. [c] Propylene concentration in toluene was calculated using the Peng−Robinson equation of state for vapor and liquid phases in equilibrium.

percentage of vinylidene, butenyl and isobutyl end groups. Chain transfer to TMA was detected experimentally and included in the kinetic model. For the first time, a kinetic model that accounts for the formation of regioirregularities, the occurrence of chain transfer to TMA, and β-hydride chain transfer to both monomer and metal is developed and parametrized through the application of systematic optimization techniques. We applied the developed kinetic model to two different catalyst systems: *rac*-Et(Ind)$_2$ZrCl$_2$/MAO (**I**/MAO) and *rac*-Et(4,7-Me$_2$-1-Ind)$_2$-ZrCl$_2$/MAO (**II**/MAO). The catalyst system **II**/MAO[26] is known to produce iPP with high isotacticity, low molecular weight, and high frequency of regioirregularities.

Results and Discussion

Polymerization Reactions. Experimental runs were performed at 40 °C in our 500 mL semibatch reactor to explore the factors of propylene partial pressure and MAO/Zr molar ratio using two different catalyst systems. For catalyst **I**/MAO, activity measured in units of kg PP/(mol Zr (M) h) increased significantly with increasing propylene partial pressure due to the increase in monomer concentration (Table 1). The amount of zirconocene was adjusted to enable a measurable reaction rate and allow for good temperature control. This adjustment should not affect the microstructure of the polymer, since it is commonly accepted that stereoregularity[27] and molecular weight distribution[15] are independent of zirconocene concentration. Activity was approximately constant with varying propylene partial pressure using **II**/MAO (Table 2; runs 9, 10, and 13). Activity increased with increasing MAO/Zr ratio for both catalysts. This fact is explained by the increasing concentration of activated complex after the catalyst/cocatalyst equilibrium reaction.[14,15] The polymerization runs in Tables 1 and 2 were used to estimate kinetic parameters for the two catalyst systems. The limited data available for parameter estimation is typical in industry where kinetic models are commonly developed from limited semi-works and manufacturing plant data.

Table 3. Estimation of Initial Percentage of Activated Complex at 40 °C

run	catalyst	MAO/Zr (mol/mol)	yield at 10 min[c] (g)	active Zr (%)
3	**I**[a]	3000	4.8	59.5
4	**I**[a]	6000	5.1	64.2
5	**I**[a]	10 000	7.3	91.6
6	**I**[a]	18 000	8.0	100.0
10	**II**[b]	1000	4.9	29.8
11	**II**[b]	8000	9.7	58.7
12	**II**[b]	15 000	16.4	100.0

[a] Runs at 2.5 atm, 4 μmol Zr. [b] Runs at 2.5 atm, 5 μmol Zr. [c] Theoretical yield calculated as the area under the reaction ratecurve in the first 10 min.

Application of mathematical modeling to the polymerization mechanism requires the measurement of the concentration of activated complex at the beginning of the reaction. A reliable analytical method to determine such concentration is nowadays a challenge, in part because the nature of the active complex remains unclear. Methods such as chemical labeling[28] and quenched flow[29] have been used. Using CH_3OT radiolabeling, Chien et al.[14] reported that two-thirds of the catalyst *rac*-Et-(4,5,6,7-H$_4$-1-Ind)$_2$ZrCl$_2$/MAO became active at 30 °C for MAO/Zr ratios larger than 3500 mol/mol. We have used an indirect method to estimate the percentage of active zirconocene for each MAO/Zr ratio at constant temperature, pressure and zirconocene concentration. Considering that after 10 min of reaction time, the reaction rates had reached a maximum and the deactivation decays were not yet significant, it was assumed that the theoretical yield after 10 min was directly proportional to the percentage of activated complex and that 100% of the catalyst was active at the highest MAO/Zr ratio (Table 3). We therefore correlated the initial concentration of activated complex with the polymer produced at the beginning of the reaction. For the catalyst **I**/MAO, at the commonly used MAO/Zr ratio of 3000 mol/mol,[25] 60% of the zirconocene molecules were active at 40 °C. The catalyst system **II**/MAO has been traditionally used with lower MAO/Zr ratios.[26,30] We estimated that 30% of **II** was active using a MAO/Zr ratio equal to 1000 mol/mol.

Polymer Microstructure and Molecular Weight. Analysis of isotacticity, regioregularity and end group structures was carried out using ^{1}H and ^{13}C NMR. The most significant chain transfer reactions for each catalyst were determined by analyzing the polymer end groups.[31,32] The predominant unsaturated end group in iPP obtained with **II**/MAO was 2-butenyl (Figure 1). The *cis*-conformation of the 2-butenyl end group was reaffirmed by ^{13}C NMR, thus indicating that *cis*-2-butenyl end groups were formed via bimolecular β-hydride transfer to the monomer after 2,1-insertion. No presence of *trans*-2-butenyl end group formed via unimolecular β-hydride transfer to the metal after a 2,1-insertion was detected.[30] The vinylidene end group, produced via β-hydride transfer after primary insertion, and *cis*-2-butenyl end group were the main unsaturations in iPP obtained using **I**/MAO (Figure 1).[25] The presence of 4-butenyl end groups was detected in each polymer.[33] Allyl end groups, formed via β-methyl transfer,[32] were detected only in iPP obtained using **II**/MAO (Figure 1), due to the steric hindrance of the 4,7-dimethyl-1-indenyl ligand.[30] The internal vinylidene structure was detected in small amounts in iPP obtained with both catalyst systems. Internal vinylidene is not considered an end group, because its formation does not necessarily involve a chain transfer reaction.[32,34,35]

Chain transfer to TMA produced an aluminum-terminated and an isobutyl-initiated chain. After washing the polymer with

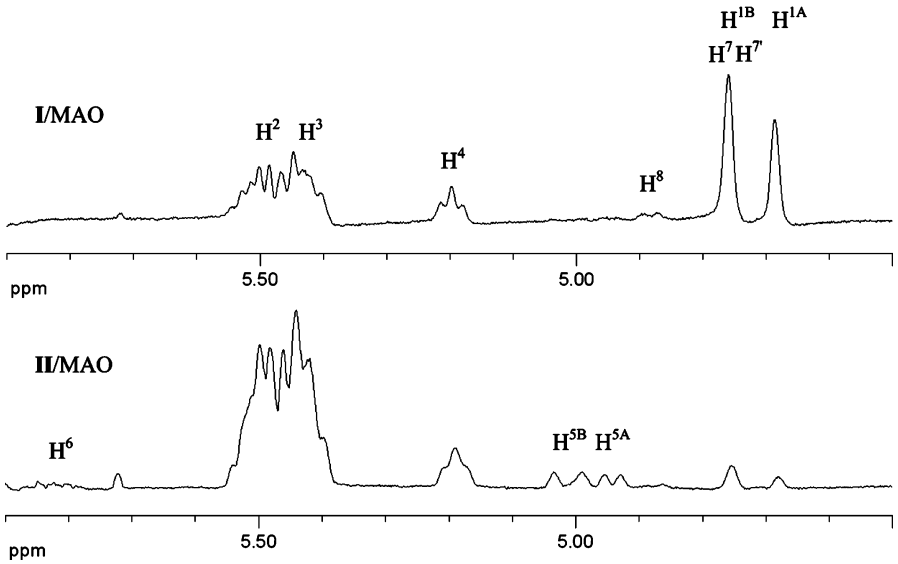

Figure 1. ^{1}H NMR olefinic region (400 MHz, TCE-d_2, 100 °C, reference C_2HDCl_4 at 5.95 ppm) of iPP obtained using **I**/MAO (run 6, 40 °C, 2.5 atm, 18 000 MAO/Zr) and **II**/MAO (run 12, 40 °C, 2.5 atm, 15 000 MAO/Zr). Proton numbering is as illustrated in Figure 3.

a methanol/HCl mixture, the aluminum-terminated chain is protonated to an isobutyl end group.[32] Figure 2 shows the increase in intensity of isobutyl end groups, detected by ^{13}C NMR (structure H in Figure 3), with increasing MAO/Zr ratio using **II**/MAO. This result is caused by the increasing rate of chain transfer to TMA contained in the MAO solution. The increase in intensity of isobutyl end groups with MAO/Zr ratio was also detected using **I**/MAO. Thus, the frequency of chain transfer to TMA was significant for both catalyst systems, producing a decreasing M_w with increasing MAO/Zr ratio (Tables 4 and 5). The intensity of *n*-butyl end groups, formed via chain transfer to TMA after a 2,1-insertion,[31,36] was not significant (Tables 4 and 5).

Characterization of regioregularity by ^{13}C NMR confirmed that 2,1-insertions were more frequent for catalyst **II** rather than **I** (Tables 4 and 5). The lower activity of catalyst **II** has been attributed to the higher frequency of secondary insertions, since it has been demonstrated that rate is lowered after a 2,1-insertion due to steric hindrance.[5,20,30,37] The high amount of 2,1-insertions also explained the lower molecular weight of the polymer produced with **II**/MAO, since it is accepted that the rate of β-hydride transfer after a 2,1-inversion is higher than after a primary insertion.[30,38] The two types of 2,1-regioirregularities, erythro and threo,[39] and 1,3-propylene insertions were detected in the microstructure of every polymer (Tables 4 and 5). As previously reported,[15] isomerization of secondary units to tetramethylene sequences (1,3 units) was enhanced when monomer concentration was lowered for both catalysts.[40,41] The ratio erythro/threo remained approximately equal with monomer concentration, and it was higher for catalyst **II** than **I**.

The catalyst system **II**/MAO was more stereospecific than **I**/MAO (Tables 4 and 5).[30] The higher isotacticity of catalyst **II** has been explained by the unfavorable, steric interaction between the methyl ligand in the 4′ position and the methyl of a primary propylene coordinated with the wrong enantioface.[42] We observed higher stereospecificity with increasing propylene concentration for both catalyst systems (Tables 4 and 5). This may be due to the competing growing-chain-end epimerization reaction.[15,27,34] The mechanism proposed for the chain-end epimerization[34] was based on the reversible formation of a zirconocene allyl dihydrogen complex. According to this pathway, high propylene concentrations would inhibit the β-agostic hydrogen interaction and allyl formation, thus increasing the isotacticity of the polymer produced.

The effect of MAO/Zr ratio on stereoselectivity was different for each catalyst system. Isotacticity increased with increasing MAO/Zr ratio using **I**/MAO (Table 4). Thus, the coordination of MAO as counterion of the activated complex appeared to improve the stereochemical control of propylene insertion.[14] The opposite trend was detected for the most stereospecific catalyst **II**/MAO (Table 5).

Kinetic Model. We recently developed a chemically based kinetic model from experimental data for slurry propylene polymerization using **I**/MAO.[25] The present study broadens the applicability of our initial model by including chain transfer to the metal (unimolecular β-hydride elimination) and chain transfer to TMA (Table 6). The inclusion of unimolecular chain transfer to the metal was necessary to model the molecular weight dependency on monomer concentration, which is determined by the competition between monomolecular and bimolecular chain transfer reactions.[8,15] A constant M_w with respect to monomer concentration indicates that bimolecular chain transfer reactions are dominant, while a linear relationship indicates that monomolecular β-hydride transfer to the metal is the dominant termination reaction.[20,25] The β-hydride transfer to the metal produces a hydride activated complex (C_H^*), which initiates a new growing chain after reactivation.[23] Chain transfer to TMA was included to describe the influence of TMA on molecular weight and the percentage of different end groups. A methylated catalyst activated complex (C_{Me}^*) is formed after chain transfer to TMA.[32] The reactivation of this catalyst complex was treated as an elementary reaction different from normal catalyst initiation because the two activated complexes are produced in different chemical environments.

The kinetic mechanism shown in Table 6 was based on the following assumptions: (i) the activated metallocene complexes act as single-center catalysts; (ii) insertion of the first monomer unit is noninstantaneous as predicted theoretically[8] and demonstrated experimentally;[6,7,10,23] (iii) deactivation of the catalyst results from unimolecular deactivation of a growing chain; (iv) secondary insertion produces a chain with a 2,1-inserted monomer, which can undergo further propagation or bimolecular β-hydride transfer to the monomer producing a *cis*-

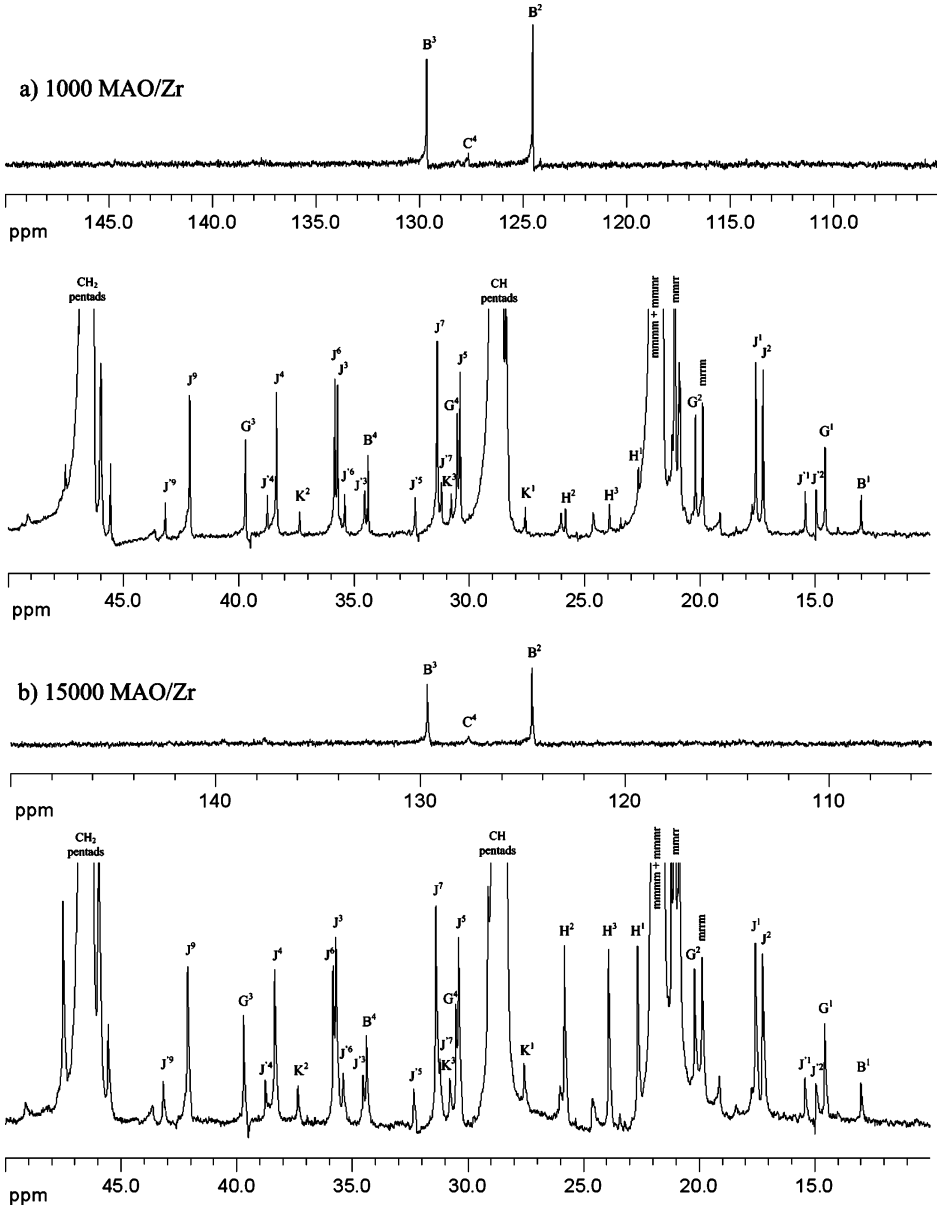

Figure 2. ^{13}C NMR spectra (151 MHz, TCE-d_2, 120 °C, reference C_2HDCl_4 at 74.26 ppm) of iPP obtained using **II**/MAO: (a) run 10, 40 °C, 2.5 atm, 1000 MAO/Zr; (b) run 12, 40 °C, 2.5 atm, 15 000 MAO/Zr. Numbering is as illustrated in Figure 3.

2-butenyl end group. Formation of 4-butenyl end groups is assumed to occur via isomerization of *cis*-2-butenyl end groups during polymerization.[33] Thus, both unsaturations are considered as butenyl end groups in the kinetic model, and (v) β-methyl chain transfer is not included due to its low occurrence with the studied catalysts. Allyl end groups represented less than 4% of the total end groups using **II**/MAO, while they were not detected in iPP produced with **I**/MAO.

Pressure was controlled to maintain a constant monomer concentration during the slurry polymerization. Assuming that monomer was consumed only in the propagation reaction (long chain approximation), the propylene flow provided a direct measurement of reaction rate as follows:[25]

$$\frac{F}{V} = k_p M L_0 \qquad (1)$$

where F is the propylene molar flow and V is reaction volume. The method of moments[25] was applied to characterize the MWD of the polymer chains, where L_n, Q_n, and U_n are the nth order moments for the distribution of active, 2,1-inserted, and dead chains, respectively:

$$L_n = \sum_{i=1}^{\infty} i^n R_i; \quad Q_n = \sum_{i=2}^{\infty} i^n P_i; \quad U_n = \sum_{i=1}^{\infty} i^n D_i \qquad (2)$$

Ordinary differential equations (ODEs) for zeroth-, first- and second-order moments of the distributions were obtained from material balances.[25] The zeroth moment for dead chains was divided into vinylidene-terminated chains $(U_0)_V$, butenyl-terminated chains $(U_0)_B$ and isobutyl-terminated chains $(U_0)_I$ to predict the percentage of each end group. Material balances for the catalyst activated complexes and TMA completed the set of differential equations defining the model, as shown in Materials and Methods. The reaction rate was calculated using eq 1. The MWD of the polymer chains was characterized by number and weight-average molecular weights calculated as follows:

$$M_n = m\frac{L_1 + Q_1 + U_1}{L_0 + Q_0 + U_0}, \quad M_w = m\frac{L_2 + Q_2 + U_2}{L_1 + Q_1 + U_1} \qquad (3)$$

Here m is the molecular weight of propylene, and $U_0 = (U_0)_V$

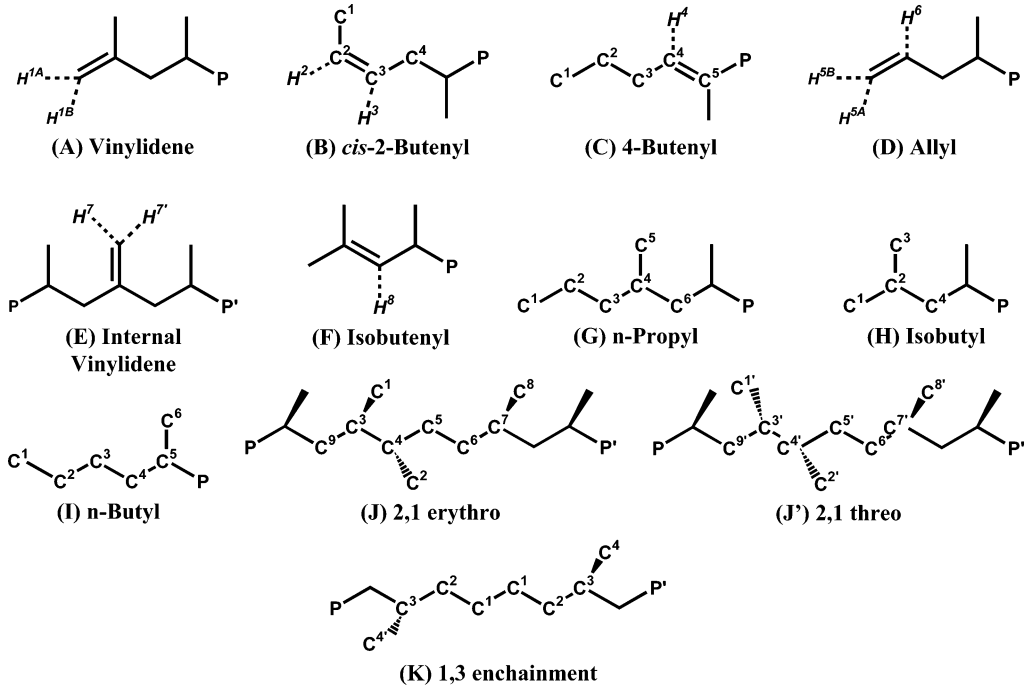

Figure 3. Proton and carbon numbering used in Figures 1 and 2, based on systems used in refs 15 and 31.

Table 4. MWD and Characterization of End Groups and Regioirregularities for Runs with I/MAO

			end groups and regioirregularities, per 10000 monomer units											
	MWD[a]		unsaturated groups					saturated groups			regioirregularities			
run	M_n (g/mol)	M_w (g/mol)	A vinylidene[b,c]	B 2-butenyl	C 4-butenyl[b]	D allyl[b]	E internal vinylidene[b]	G *n*-propyl	H isobutyl	I *n*-butyl	J 2,1 erythro	J′ 2,1 threo	K 1,3	tacticity[f] (% mmmm)
1	7922	16326	4.9	3.9	0.7	n.d.[d]	0.4	15.7	30.9	n.d.	20.6	12.3	15.5	82.0
2	9815	21015	4.3	3.9	0.9	n.d.	0.5	12.5	17.9	n.d.	24.9	12.8	11.2	83.1
3	13895	29852	5.8	7.2	1.4	n.d.	1.3	16.4	6.1	trace[e]	35.7	18.6	9.9	87.7
4	12837	28436	3.1	4.9	1.2	n.d.	0.7	18.1	6.3	trace	39.4	22.3	6.9	87.5
5	12309	26759	2.5	3.8	1.1	n.d.	0.7	9.9	5.9	trace	29.9	16.0	5.7	88.3
6	10882	22959	1.9	3.3	1.1	n.d.	0.6	9.6	7.3	trace	31.1	18.1	6.3	89.3
7	17256	36031	2.4	5.1	0.9	n.d.	0.6	13.0	3.4	trace	37.4	20.1	4.4	88.2
8	18586	39936	3.7	5.7	1.5	n.d.	0.7	15.0	3.9	n.d.	41.4	23.2	4.1	87.0

[a] Measured by GPC. [b] Quantified relative to 2-butenyl multiplet in ^{1}H NMR spectra. [c] Sum of vinylidene and isobutenyl (F) produced from vinylidene during polymer analysis. [d] n.d.: not detected. [e] Trace: signal under limit of detection of ^{13}C NMR, ca. 2/10 000 monomer units. [f] Calculated according to ref 15, based on enantiomorphic site control model.

Table 5. MWD and Characterization of End Groups and Regioirregularities for Runs with II/MAO

			end groups and regioirregularities, per 10000 monomer units											
	MWD[a]		unsaturated groups					saturated groups			regioirregularities			
run	M_n (g/mol)	M_w (g/mol)	A vinylidene[b,c]	B 2-butenyl	C 4-butenyl[b]	D allyl[b]	E internal vinylidene[b]	G *n*-propyl	H isobutyl	I *n*-butyl	J 2,1 erythro	J′ 2,1 threo	K 1,3	tacticity[f] (% mmmm)
9	6244	12873	1.8	29.9	7.1	2.0	0.7	47.1	20.8	trace[e]	100.8	23.6	14.8	91.9
10	6086	12584	0.8	44.6	5.7	1.6	0.5	50.7	15.0	n.d.[d]	110.6	27.2	7.6	92.1
11	4032	8822	0.6	40.6	3.7	1.5	0.3	53.9	61.6	trace	108.7	26.7	13.3	91.0
12	3471	7502	0.8	43.5	7.5	1.7	0.6	62.0	109.7	n.d.	129.3	26.4	12.6	89.0
13	6316	13039	0.9	41.4	5.0	1.5	0.5	49.9	8.1	n.d.	100.2	25.7	6.8	92.6

[a] Measured by GPC. [b] Quantified relative to 2-butenyl multiplet in ^{1}H NMR spectra. [c] Sum of vinylidene and isobutenyl (F) produced from vinylidene during polymer analysis. [d] n.d.: not detected. [e] Trace: signal under limit of detection of ^{13}C NMR, ca. 2/10 000 monomer units. [f] Calculated according to ref 15, based on enantiomorphic site control model.

$+ (U_0)_B + (U_0)_I$. The kinetic model describes the formation of vinylidene-, butenyl-, and isobutyl-terminated chains. The percentages of butenyl (B) and isobutyl end groups (I) relative to the total number of end groups was calculated as follows:

$$B = 100 \times \frac{(U_0)_B}{(U_0)_V + (U_0)_B + (U_0)_I},$$

$$I = 100 \times \frac{(U_0)_I}{(U_0)_V + (U_0)_B + (U_0)_I} \quad (4)$$

Estimation of Kinetic Parameters. The kinetic rate constants were estimated for each catalyst system at 40 °C using on-line reaction rate data and end-of-batch measurements of MWD and the percentages of end groups. The estimation strategy involved the decomposition of the least-squares optimization problem into two sequential subproblems, as explained in Materials and Methods.[23,25] The first subproblem was formulated to minimize the least-squares difference between experimental and predicted reaction rate trajectories. Runs 1, 2, 3, and 7 for **I**/MAO (Table 1) and runs 9, 10, and 13 for **II**/MAO (Table 2) were used in

Table 6. Kinetic Model

Kinetic Model	
initiation	$C^* + M \xrightarrow{k_{in}} R_1$
propagation	$R_i + M \xrightarrow{k_p} R_{i+1}$
chain deactivation	$R_i \xrightarrow{k_d} D_i + C_d^*$
chain transfer to monomer	$R_i + M \xrightarrow{k_M} D_i + R_1$
chain transfer to metal	$R_i \xrightarrow{k_H} C_H^* + D_i$
reactivation after transfer to metal	$C_H^* + M \xrightarrow{k_{rH}} R_1$
secondary (2,1) insertion	$R_i + M \xrightarrow{k_s} P_{i+1}$
propagation after 2,1-insertion	$P_i + M \xrightarrow{k_{sp}} R_{i+1}$
chain transfer after 2,1-insertion	$P_i + M \xrightarrow{k_{sM}} D_i + R_1$
chain transfer to TMA	$R_i + TMA \xrightarrow{k_{Al}} C_{Me}^* + D_i$
reactivation after transfer to TMA	$C_{Me}^* + M \xrightarrow{k_{rAl}} R_i$

Species

C^* = catalyst activated complex
M = monomer
R_i = active chain with "*i*" monomer units
D_i = dead chain with "*i*" monomer units
C_d^* = inactive catalyst complex
P_i = 2,1-inserted chain with "*i*" monomer units
C_H^* = hydride catalyst activated complex
C_{Me}^* = methyl catalyst activated complex
TMA = trimethylaluminum

Table 7. Kinetic Rate Constants for Catalyst Systems I/MAO and II/MAO at 40 °C Estimated from Reaction Rate, MWD, and Percentage of End Group Data

catalyst	k_{in} (L mol^{-1} s^{-1})	k_p (L mol^{-1} s^{-1})	k_d (s^{-1})	k_M (L mol^{-1} s^{-1})	k_H (s^{-1})	k_{rH}[a] (L mol^{-1} s^{-1})	k_s (L mol^{-1} s^{-1})	k_{sp} (L mol^{-1} s^{-1})	k_{sM}[a] (L mol^{-1} s^{-1})	k_{Al} (L mol^{-1} s^{-1})	k_{rAl}[a] (L mol^{-1} s^{-1})
I	1.78E−05	3.76E+04	9.62E−03	1.26E+01	2.65E+01	>4.2E+03	4.94E+01	0	>6.7E+03	1.97E+03	>1.0E+03
II	6.03E−05	1.70E+04	8.06E−03	9.13E−01	4.16E−01	>4.2E+01	9.74E+01	0	>3.3E+03	5.46E+03	>7.2E+03

[a] Values greater than that reported changed the absolute value of the combined objective function by less than 10^{-3}.

the first subproblem. Reaction rate data used to estimate the percentage of activated catalyst were not included in the optimization. The second subproblem was formulated to minimize the least-squares difference between experimental and predicted end-of-batch data for molecular weights and the percentages of end groups. Runs 1−7 for **I**/MAO and runs 9−13 for **II**/MAO were used in the second optimization subproblem. A final optimization involving weighted versions of the two least-squares objective functions was performed using the results of the subproblems as initial parameter values. Reaction rate and end-of-batch data from run 8 (Table 1) were used to validate the predictive capabilities of the kinetic model.

The final values of the estimated kinetic rate constants for each catalyst system at 40 °C are shown in Table 7. As reported in our previous study,[25] the inclusion of the propagation reaction after a 2,1-insertion neither improved the prediction of reaction rate data nor the end-of-batch measurements. This suggests that 2,1-inserted chains produced butenyl-terminated chains via β-hydride transfer after secondary insertion. For both catalysts, a very large value of k_{sM} relative to k_s was obtained and k_{sp} was equal to zero. The optimal solutions also predicted fast reactivation reactions after β-hydride transfer to the metal and chain transfer to TMA. The large rate constants were necessary to eliminate the influence of the two chain transfer reactions on reaction rate. If the rates of reactivation were the same order of magnitude as the initiation rate, the occurrence of chain transfer to metal and TMA would slow the reaction rate dramatically. Quantum mechanical studies in metallocene-catalyzed ethylene polymerization predicted a high activation barrier (close to 20 kcal/mol) for unimolecular β-hydride transfer to the metal, while the produced hydride metallocene complex was predicted to be very unstable.[4,43,44] Density functional calculations on polyethylene chain transfer to TMA with the catalyst Cp_2ZrCl_2/MAO predicted that the produced Cp_2ZrMe^+ cation was particularly unstable.[45] The large rate constants obtained for reactivation after chain transfer to metal (k_{rH}) and chain transfer to TMA (k_{rAl}) relative to k_H and k_{Al} were in accordance with these computational studies.

Effects on Reaction Rate. Model predictions of reaction rate captured the typical behavior of experimental rate profiles for metallocene-catalyzed polymerizations in semibatch reactors (Figures 4−7).[9,10,14,23,46] The activation period was modeled by the noninstantaneous insertion of the first monomer unit. Solution of the parameter estimation problem showed that the initiation reaction was the rate-limiting step in the mechanism, as shown by the low value of k_{in} (Table 7). Figures 4 and 5 show the influence of propylene partial pressure on reaction rate for catalysts **I**/MAO and **II**/MAO, respectively. The model captured the increasing reaction rate with increasing pressure due to the higher propylene concentration in solution. Also, the model predicted more pronounced deactivation decays with increasing monomer concentration (Figures 4 and 5).[25] The catalyst system **I**/MAO produced a higher reaction rate than **II**/MAO at the same conditions, as reflected by the relative k_p values (Table 7).

The reaction rate increases with increasing MAO/Zr ratio for both catalyst systems (Figures 6 and 7). Larger MAO/Zr ratios shifted the activation equilibrium between catalyst and cocatalyst to produce higher concentrations of activated complex at the beginning of the reaction (C_0^*). Because the model uses C_0^* as a scaling factor for the reaction rate profiles, the influence of MAO/Zr ratio on the deactivation decay cannot be predicted. For both catalysts, the experimental reaction rate profiles had

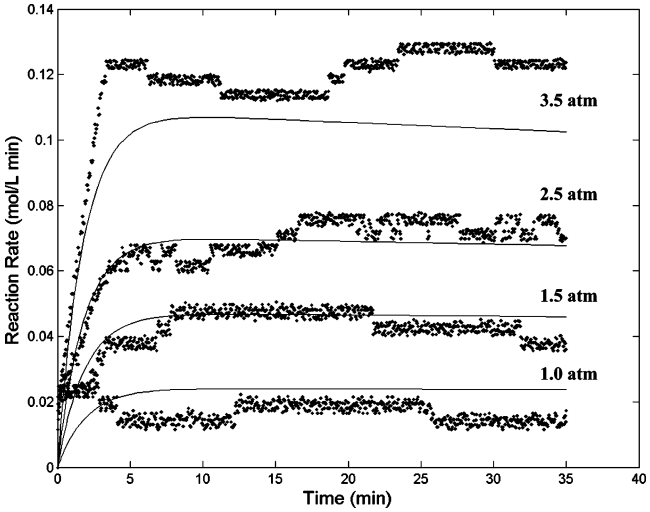

Figure 4. Experimental (scattered line) and predicted (solid line) reaction rate using **I**/MAO at 40 °C, 3000 MAO/Zr and four partial pressures of propylene: 1.0, 1.5, 2.5, and 3.5 atm (runs 1, 2, 3, and 7).

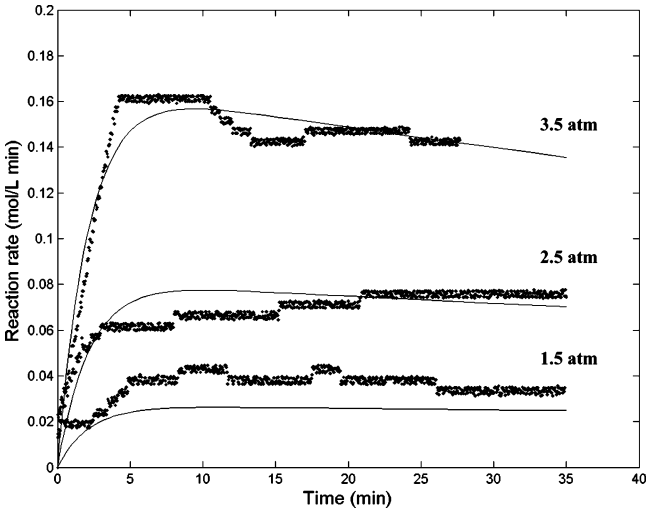

Figure 5. Experimental (scattered line) and predicted (solid line) reaction rate using **II**/MAO at 40 °C, 1000 MAO/Zr and three partial pressures of propylene: 1.5, 2.5, and 3.5 atm (runs 9, 10, and 13).

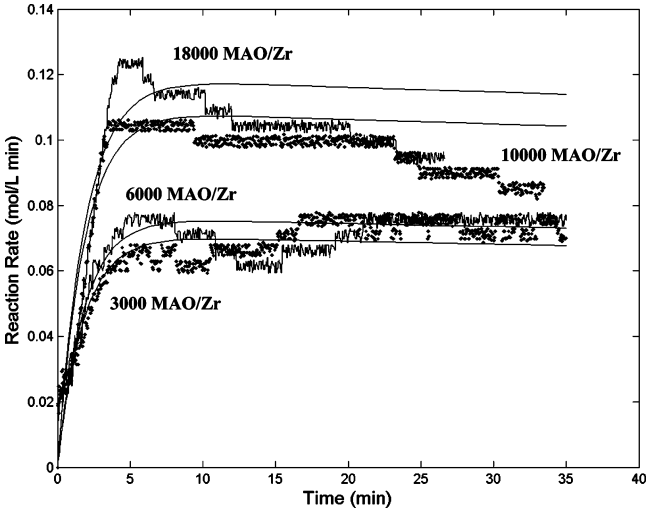

Figure 6. Experimental (scattered line) and predicted (solid line) reaction rate using **I**/MAO at 40 °C, 2.5 atm and four MAO/Zr ratios: 3000, 6000, 10 000, and 18 000 mol/mol (runs 3, 4, 5, and 6).

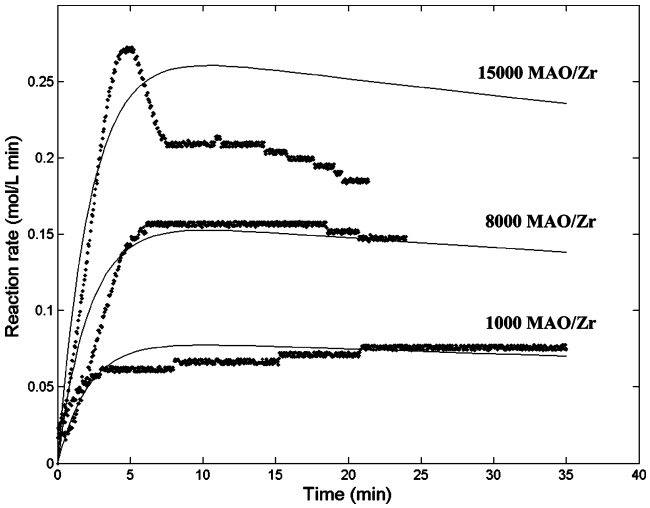

Figure 7. Experimental (scattered line) and predicted (solid line) reaction rate using **II**/MAO at 40 °C, 2.5 atm and three MAO/Zr ratios: 1000, 8000, and 15 000 mol/mol (runs 10, 11, and 12).

more pronounced deactivation decays at large MAO/Zr ratios (Figures 6 and 7). This result may be explained by an unmodeled deactivation reaction involving residual TMA, since it has been observed that the addition of free TMA decreases catalyst activity.[14] The sharp maximum in reaction rate observed in run 10 (Figure 7, 15 000 MAO/Zr) was caused by a temperature overshoot of 2 °C in the first 5 min of reaction. This run emphasizes the importance of tight temperature control in the measurement of polymerization kinetics.

For the validation run performed with **I**/MAO at the highest propylene partial pressure (4 atm), the model exhibited substantial disagreement with the measured reaction rate (Figure 8). Experimental variability in the reaction rate measurement was always present due to the large influence that impurities, such as oxygen and water, had on the polymerization kinetics. However, the large difference between predicted and experimental results was more likely due to the simplified nature of the model, which neglects the occurrence of stereodefects by chain-end epimerization.[27,34,47] We detected decreasing isotacticity with increasing monomer concentration, which can be explained by epimerization (Tables 4 and 5). In a simple model with different propagation rate constants for each epimerization state, a propagation rate law with an exponential dependence on propylene concentration has been generated.[15,34] Thus, the exclusion of epimerization from our model may explain the poor prediction of reaction rate at the highest pressure. The inclusion of the chain-end epimerization reaction in our kinetic model would require broadening the experimental range of monomer concentrations to be able to estimate the reactivity and stereoselectivity of each epimerization state as well as measurement of the distribution of pentads.[48,49] Such an extension is outside the scope of this paper.

Effects on MWD and End Groups. The agreement between predicted and experimental results for the MWD are shown in Table 8. The M_w for polymer produced with **II**/MAO was lower than that for **I**/MAO (Figures 9 and 10). This result is explained by the higher frequency of 2,1-inserted chain formation with catalyst **II**/MAO ($k_s = 97.4$ L mol^{-1} s^{-1} vs $k_s = 49.4$ L mol^{-1} s^{-1} for **I**/MAO) because the model predicted fast chain transfer to monomer for 2,1-inserted chains. The dependency of M_w on monomer concentration was different for each catalyst system (Figure 9). The increasing trend for catalyst **I**/MAO was the result of monomolecular β-hydride transfer to the metal (k_H) competing with bimolecular chain transfer to monomer after primary insertion (k_M) and 2,1-insertion (k_{sM}). For **II**/MAO, the rate constant for monomolecular transfer to metal was small

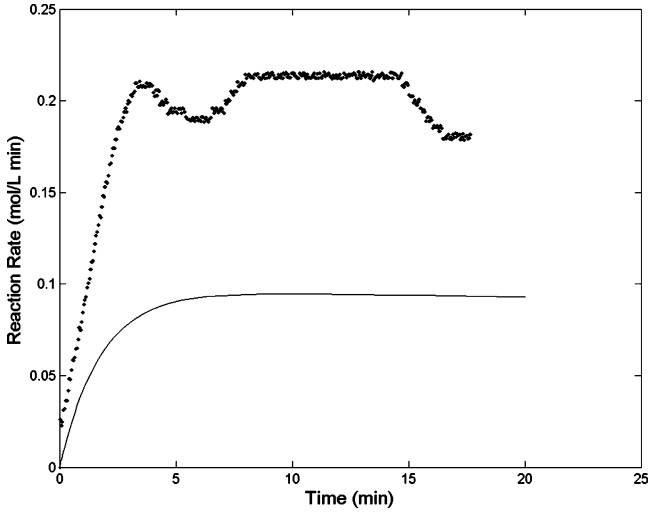

Figure 8. Experimental (scattered points) and predicted (solid line) reaction rate using **I**/MAO at 40 °C, 4.0 atm, and 3000 MAO/Zr. This experimental run was not used to estimate kinetic parameters.

Table 8. Experimental and Predicted Results for Molecular Weight Distribution

		experimental[a]			kinetic model		
run	catalyst	M_n (g/mol)	M_w (g/mol)	PDI	M_n (g/mol)	M_w (g/mol)	PDI
1	**I**	7922	16 326	2.06	7196	14 333	1.99
2	**I**	9815	21 015	2.14	10 549	21 030	1.99
3	**I**	13 895	29 852	2.15	16 055	32 027	1.99
4	**I**	12 837	28 436	2.22	14 000	27 923	1.99
5	**I**	12 309	26 759	2.17	12 070	24 072	1.99
6	**I**	10 882	22 959	2.11	9423	18 790	1.99
7	**I**	17 256	36 031	2.09	18 637	37 184	2.00
8[b]	**I**	18 586	39 936	2.15	19 831	39 569	2.00
9	**II**	6244	12 873	2.06	5833	11 564	1.98
10	**II**	6086	12 584	2.07	6487	12 866	1.98
11	**II**	4032	8822	2.19	4098	8322	2.03
12	**II**	3471	7502	2.16	3560	7712	2.17
13	**II**	6316	13 039	2.06	6787	13 462	1.98

[a] Measured by GPC. [b] Run not included in the estimation of parameters.

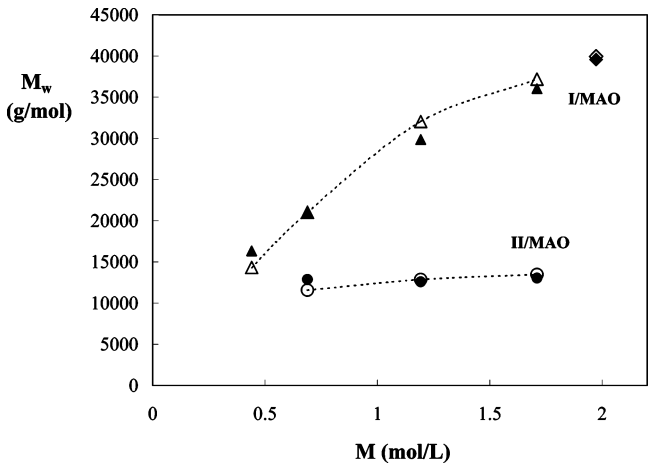

Figure 9. Experimental (scattered points) and predicted (solid line) M_w vs monomer concentration with **I**/MAO (runs 1, 2, 3, and 7) and **II**/MAO (runs 9, 10, and 13). Model prediction (◆) and experimental (◇) M_w for run 8 is also shown.

($k_H = 0.42\ s^{-1}$ vs $k_H = 26.5\ s^{-1}$ for **I**/MAO), resulting in only a slight increase of M_w with monomer concentration due to the predominant bimolecular transfer to the monomer after 2,1-insertion. Both catalysts exhibited a decreasing M_w with increasing concentration of TMA contained in the MAO solution (Figure 10). The model reproduced the measured M_w trend for

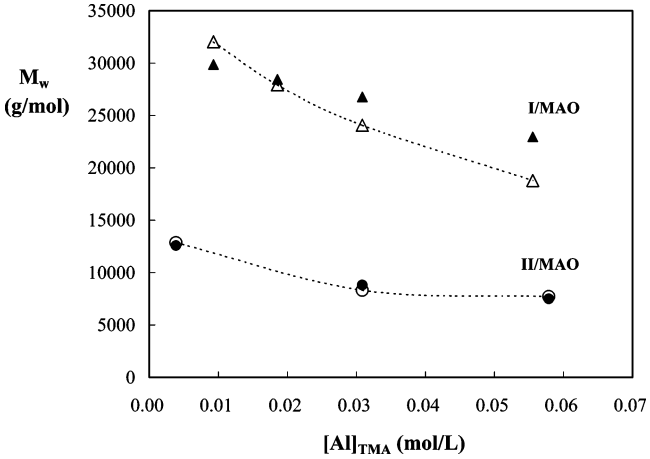

Figure 10. Experimental (scattered points) and predicted (solid line) M_w vs TMA concentration with **I**/MAO (runs 3, 4, 5, and 6) and **II**/MAO (runs 10, 11, and 12).

II/MAO, but overestimated the rate of transfer to TMA for **I**/MAO (Figure 10). Chain transfer to TMA was more significant for **II**/MAO than for **I**/MAO, as expressed by the relative values of k_{Al} (Table 7).

An interesting feature of the modeling results regards the polymer polydispersity. The model predicted a Schulz−Flory distribution with a polydispersity close to 2 for the majority of runs (Table 8). However, runs 11 and 12 with a high frequency of chain transfer to TMA showed an increasing polydispersity due to the depletion of TMA during the batch polymerization. The variable TMA concentration produced chains with a broader range of molecular weights, thereby more strongly affecting polymer MWD for **II**/MAO due to more significant chain transfer to TMA. Experimental polydispersities obtained with **II**/MAO were in agreement with this observation. Propylene diffusion limitations may explain deviations from the theoretical value of 2 for measured polydispersities with **I**/MAO.[48]

The increasing percentage of butenyl end groups with increasing monomer concentration reaffirmed that β-hydride transfer after 2,1-insertion was monomer-dependent (Figure 11).[15,30] As a consequence, chain transfer to TMA was enhanced at low monomer concentrations due to the lower frequency of chain transfer to monomer reactions.[20] The percentage of isobutyl end groups produced with **II**/MAO was lower than that for **I**/MAO due to the lower MAO/Zr ratios used (Figure 11). Disagreement between the experimental and predicted percentages of vinylidene and isobutyl end groups was observed for runs at low monomer concentrations using **I**/MAO. This result may be attributed to the increasing concentration of zirconocene needed to generate measurable reaction rates with this catalyst. This resulted in the overestimation of the transfer rate to TMA observed for catalyst **I**/MAO (Figures 10 and 12). The increasing percentage of isobutyl end groups with increasing TMA concentration was captured by the model for both catalysts (Figure 12). Results from the kinetic model are compared to experimental data for the percentages of end groups in Table 9. For the case of polymer produced with **II**/MAO, the percentage of isobutyl-terminated chains increased to 52% and the number-average molecular weight decreased to 3500 g/moL. Thus, changing reaction conditions was found to be a promising method for producing aluminum-terminated iPP. The model was used as a purely predictive tool for the run at 4 atm of pressure with catalyst **I**/MAO. The model predictions for the molecular weight and percentage of end groups were very accurate as shown in Figures 9 and 11.

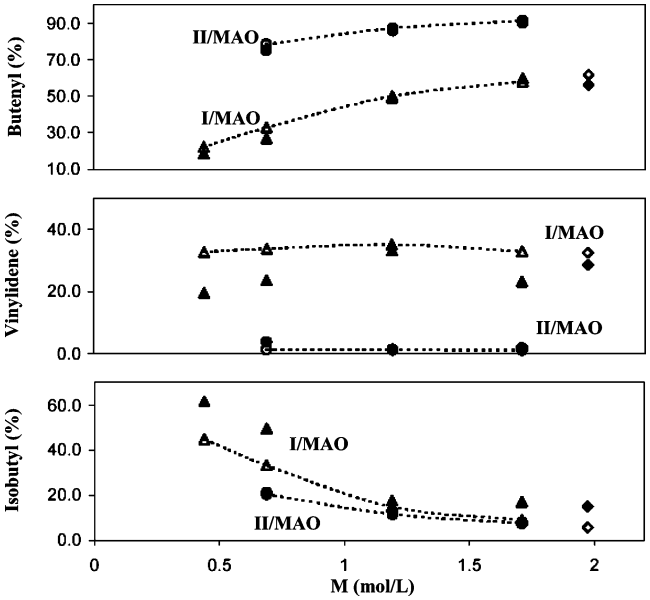

Figure 11. Experimental (scattered points) and predicted (solid line) percentages of end groups vs monomer concentration for catalyst systems **I**/MAO (runs 1, 2, 3, and 7) and **II**/MAO (runs 9, 10, and 13). Model prediction (◆) and experimental (◇) percentages of end groups for run 8 are also shown.

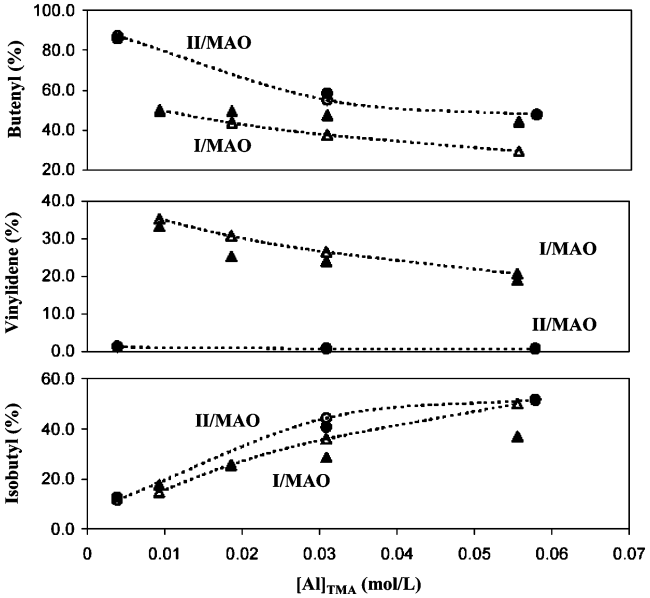

Figure 12. Experimental (scattered points) and predicted (solid line) percentages of end groups vs TMA concentration for catalyst systems **I**/MAO (runs 3, 4, 5, and 6) and **II**/MAO (runs 10, 11, and 12).

Conclusions

Monomolecular β-hydride transfer to metal and chain transfer to TMA reactions were added to our previously developed kinetic model for the zirconocene-catalyzed slurry polymerization of propylene.[25] For the first time, a kinetic model was able to predict the effect of MAO/Zr ratio on reaction rate, MWD and percentage of end groups in the metallocene-catalyzed propylene polymerization. Following systematic estimation of the kinetic parameters, the kinetic model was successfully applied to the catalyst systems *rac*-Et(Ind)$_2$ZrCl$_2$/MAO (**I**/MAO) and *rac*-Et(4,7-Me$_2$-1-Ind)$_2$ZrCl$_2$ (**II**/MAO).

The model captured the effect of monomer concentration and MAO/Zr ratio on reaction rate. The estimation of the concentration of activated complex at the beginning of the reaction enabled the model to predict higher reaction rates with increasing MAO/Zr ratio. However, the model was not capable of predicting the more pronounced deactivation decays at high MAO/Zr ratios. To account for this effect, a deactivation reaction involving residual TMA should be included in future modeling work. Contrary to previously developed models,[6−10,23] our model included a comprehensive set of chain transfer reactions that zirconocene catalysts undergo during propylene polymerization. This allowed the prediction of molecular weights and percentages of end groups using two different catalyst complexes. The M_w of polymer produced with **II**/MAO was lower than for **I**/MAO. This result was modeled with the higher frequency of 2,1-inserted chains formation for the catalyst **II**/MAO, since a 2,1-inserted chain was forced to undergo chain transfer to monomer producing a *cis*-2-butenyl-terminated chain. The M_w of polymer produced with **I**/MAO increased with monomer concentration. This trend was modeled with a high rate of monomolecular β-hydride transfer to the metal ($k_H = 26.5\ s^{-1}$) for **I**/MAO. Chain transfer to TMA was more significant for catalyst **II**/MAO ($k_{Al} = 5.46 \times 10^{+3}$ L mol^{-1} s^{-1}) than for **I**/MAO ($k_{Al} = 1.97 \times 10^{+3}$ L mol^{-1} s^{-1}). For both catalysts, increasing concentration of residual TMA reduced the M_w of the polymer by producing more isobutyl-terminated chains.

The optimal solution was more accurate for catalyst **II**/MAO compared to **I**/MAO. This may be due to several reasons: (i) the same amount of catalyst was used for each run; (ii) smaller number of runs were performed to capture the experimental trends with propylene partial pressure and MAO/Zr ratio; (iii) measurements of percentage of end groups by NMR were more accurate because of the lower polymer molecular weight. The use of the developed kinetic model as a predictive tool was tested for the run at the highest pressure using **I**/MAO. The model accurately predicted the molecular weight and percentage of end groups for the polymer produced. However, it did not succeed in the prediction of the reaction rate. The inclusion of chain-end-epimerization in a two-state model may increase the predictive capability of reaction rate in future investigations.

The variation of polymerization conditions was proven to effectively change the M_w and the percentages of end groups in the polymer produced. This strategy has potential application in the production of highly isotactic, low molecular weight polypropylene with aluminum-terminated chains, which could be used to attach functional groups to the chain-end or in the production of block copolymers.

Table 9. Experimental and Predicted Results for Percentages of End Groups Assuming the Formation of Only Vinylidene, Isobutyl and Butenyl End Groups

		experimental[a]			kinetic model		
run	catalyst	vinylidene (%)	butenyl[b] (%)	isobutyl[c] (%)	vinylidene (%)	butenyl[b] (%)	isobutyl[c] (%)
1	**I**	19.6	18.7	61.6	32.8	22.3	44.8
2	**I**	23.6	26.9	49.5	33.9	32.8	33.3
3	**I**	33.2	49.2	17.6	35.2	50.0	14.8
4	**I**	25.2	49.4	25.4	30.7	43.6	25.7
5	**I**	24.0	47.4	28.6	26.4	37.6	36.0
6	**I**	18.9	44.2	36.9	20.6	29.3	50.1
7	**I**	23.2	59.8	17.0	33.0	58.1	8.9
8[d]	**I**	28.6	56.3	15.1	32.5	61.8	5.7
9	**II**	3.7	75.1	21.1	1.2	78.4	20.3
10	**II**	1.4	85.9	12.8	1.1	87.3	11.5
11	**II**	0.8	58.5	40.7	0.7	54.9	44.3
12	**II**	0.8	47.8	51.5	0.6	47.7	51.7
13	**II**	1.8	90.4	7.9	1.1	91.4	7.5

[a] Measured by ^{1}H and ^{13}C NMR. [b] Sum of *cis*-2-butenyl and 4-butenyl end groups. [c] One-half of the isobutyl groups are end groups, since one isobutyl-initiated and one isobutyl-terminated chains are formed in chain transfer to TMA. [d] Run not included in the estimation of parameters.

Materials and Methods

Materials. The metallocene complex *rac*-Et(Ind)$_2$ZrCl$_2$, triisobutylaluminum (TIBA) 1.0 M solution in toluene were purchased from Sigma-Aldrich. The compound *rac*-Et(4,7-Me$_2$-1-Ind)$_2$ZrCl$_2$ was provided by Dr. Luigi Resconi (Basell Polyolefins, Ferrara, Italy) as a mixture of 90% *rac* and 10% *meso* enantiomers. Methylaluminoxane (MAO) 30wt % solution in toluene was donated by Albemarle Corp. (Baton Rouge, LA). The metallocene reactants, MAO and TIBA were used without further purification. Toluene purchased from Sigma-Aldrich was dried over sodium and distilled. Propylene (polymer grade, 99.95% pure) and nitrogen (prepurified grade) were supplied by Airgas, Inc. Molecular sieves (3 Å) from Sigma-Aldrich (St Louis, MO), Selexsorb COS (Alcoa World Chemicals, Houston, TX) and nonactivated cuprous oxide (Engelhard Co., Iselin, NY) were used as adsorbents to purify the propylene.

Semibatch Reactor. The semibatch reactor was an Autoclave Engineers 500 mL ZipperClave. Propylene flow was measured by a Sierra Instruments Side Track 840 Series mass flow controller (0−5000 cm^3/min of air at 70 °F and 1 atm). A magnetically driven 45°-pitched 4-blade turbine with a maximum speed of 3000 rpm mixed the reactor medium. Pressure, gas flow and agitator speed were automatically controlled using a National Instruments LabView software Virtual Instrument, interfaced to a Koyo model 250 Programmable Logic Controller with a 205 model CPU to handle all analog/digital inputs and outputs.

A Julabo FP50 MV Heating/Cooling System was used as a thermostatic bath with Thermal H5S fluid as heat transfer medium (−20 to +120 °C). The reactor temperature was monitored using a K-type thermocouple and regulated using a cascade control structure. The primary regulator was coded in the computer interface (LabView 5.1) as a proportional-integral-derivative (PID) controller cascaded to the secondary PID controller available in the Julabo FP50 MV. The primary controller computed a set point signal for the secondary controller by comparing the reactor temperature with its set point. The secondary controlled regulated the oil temperature in the Julabo FP50 MV by manipulating the heat supply of the bath. A dynamic simulation of the cascade control system and the reactor energy balance developed in Simulink (Mathworks, Natick, MA) was used to find the best set of PID tuning parameters for the primary controller. In a typical reaction, the temperature set point was set 1.5 °C below the target temperature at time zero to avoid overshoot in the reactor temperature at the beginning of the reaction. A logic circuit was implemented to switch the temperature set point to 40 °C when the heat of reaction raised the reactor temperature above 40 °C. This control strategy allowed the reactor to maintain the temperature within ±1 °C of the target value during most polymerizations. An exception was run 12, where the higher catalyst activity raised the temperature to 42 °C at the beginning of the reaction.

Polymerization Procedure. The day before a typical polymerization reaction, the reactor was heated to 80 °C while a flow of prepurified nitrogen (2500 cm^3/min) was purged for 2 h to remove water and oxygen. The reactor was subject to a pressure test at room-temperature overnight to check for leaks. The day of the reaction, the reactor was loaded with 200 mL of toluene and 0.6 mL of 1.0 M triisobutyl aluminum (TIBA), which acted as a scavenger. The system was heated to the desired temperature and the toluene was saturated with propylene at the desired pressure while the reactor was stirred at 1250 rpm. The reaction was started with the injection of the catalyst/MAO mixture, which had been premixing for 30 min in dry atmosphere to ensure that the contacted catalyst was in form of active species.[10] Temperature was generically controlled to be at the set point within ±1 °C during polymerization. The reaction was finished by stopping the monomer gas flow, injecting 10 mL of methanol and degassing the reactor. The product was washed overnight with a methanol/hydrochloric acid mixture (10:1% vol.) and dried under vacuum for 12 h. The percentage of solids at the end of the runs never exceeded 19%, minimizing monomer diffusion limitations.

Characterization Methods. The molecular weight distribution of the polypropylenes was measured by gel permeation chromatography as previously published.[25] Polymer end groups were analyzed by high temperature ^{1}H and ^{13}C NMR spectroscopy. ^{1}H NMR analysis was performed using a Bruker AVANCE 400 NMR spectrometer at 100 °C and 1,1,2,2-tetrachloroethane-d_2 as solvent.[25] A Bruker AVANCE D600 FT NMR spectrometer operating at 151 MHz and 120 °C was used to perform ^{13}C NMR analysis. Samples were prepared in a 10 mm probe dissolving 350 mg of polymer in 2 mL of 1,1,2,2-tetrachloroethane-d_2. Instrument conditions were as follows: pulse angle, 90°; acquisition time, 1.5 s; delay time, 6.5 s; spectral width, 31 746 Hz; number of scans, 1200.

Kinetic Model Equations. The ordinary differential equations for zeroth-, first- and second-order moments of the distribution of active, 2,1-inserted, and dead chains are

$$\frac{dL_0}{dt} = k'_{in}C^* - (k_d + k_H + k'_s + k_{Al}TMA)L_0 + (k'_{sp} + k'_{sM})Q_0 + k'_{rH}C^*_H + k'_{rAl}C^*_{Me} \quad (5)$$

$$\frac{dL_1}{dt} = k'_{in}C^* + k'_pL_0 - (k_d + k_H + k'_s + k_{Al}TMA)L_1 + k'_M(L_0 - L_1) + k'_{sp}(Q_0 + Q_1) + k'_{sM}Q_0 + k'_{rH}C^*_H + k'_{rAl}C^*_{Me} \quad (6)$$

$$\frac{dL_2}{dt} = k'_{in}C^* + k'_p(L_0 + 2L_1) - (k_d + k_H + k'_s + k_{Al}TMA)L_2 + k'_M(L_0 - L_2) + k'_{sp}(Q_0 + 2Q_1 + Q_2) + k'_{sM}Q_0 + k'_{rH}C^*_H + k'_{rAl}C^*_{Me} \quad (7)$$

$$\frac{dQ_0}{dt} = k'_sL_0 - (k'_{sp} + k'_{sM})Q_0 \quad (8)$$

$$\frac{dQ_1}{dt} = k'_s(L_0 + L_1) - (k'_{sp} + k'_{sM})Q_1 \quad (9)$$

$$\frac{dQ_2}{dt} = k'_s(L_0 + 2L_1 + L_2) - (k'_{sp} + k'_{sM})Q_2 \quad (10)$$

$$\frac{d(U_0)_V}{dt} = (k_d + k_H + k'_M)L_0 \quad (11)$$

$$\frac{d(U_0)_B}{dt} = k'_{sM}Q_0 \quad (12)$$

$$\frac{d(U_0)_I}{dt} = k_{Al}TMAL_0 \quad (13)$$

$$\frac{dU_1}{dt} = (k_d + k_H + k'_M + k_{Al}TMA)L_1 + k'_{sM}Q_1 \quad (14)$$

$$\frac{dU_2}{dt} = (k_d + k_H + k'_M + k_{Al}TMA)L_2 + k'_{sM}Q_2 \quad (15)$$

where $k' = kM$. Material balances for the catalyst activated complexes and TMA are

$$\frac{dC^*}{dt} = -k'_{in}C^* \quad (16)$$

$$\frac{dC^*_H}{dt} = k_HL_0 - k'_{rH}C^*_H \quad (17)$$

$$\frac{dTMA}{dt} = -k_{Al}TMAL_0 \quad (18)$$

$$\frac{dC^*_{Me}}{dt} = k_{Al}TMAL_0 - k'_{rAl}C^*_{Me} \quad (19)$$

The kinetic model composed of eqs 5−19 was solved numerically using the following initial conditions: $L_0 = L_1 = L_2 = 0$; $Q_0 = Q_1 = Q_2 = 0$; $U_0 = U_1 = U_2 = 0$; $C^* = C^*_0$; $TMA = TMA_0$ and $C^*_H = C^*_{Me} = 0$.

Parameter Estimation Procedure. Estimation of the kinetic parameters was performed by decomposing the full optimization problem into two sequential subproblems. Each catalyst system was treated separately to generate a unique set of kinetic rate constants. The reaction rate was assumed to be mainly affected by the initiation, propagation and deactivation reactions. Thus, k_{in}, k_p, and k_d were estimated from reaction rate data by minimizing the following least-squares objective function:

$$\min_{\theta_1} \sum_{i=1}^{N_i} \sum_{j=1}^{N_j} [p^i(t_j) - \hat{p}^i(t_j)]^2 \tag{20}$$

where $p^i(t_j)$ represents the measured polymerization rate at time t_j for run i, the "$\wedge$" denotes a predicted value obtained from the kinetic model, N_j is the total number of data points for the ith run, and N_i is the total number of runs. The kinetic parameters $\theta_1 = \{k_{in}, k_p, k_d\}$ served as decision variables in the first optimization subproblem, while the remaining kinetic rate constants were set to reasonable values.

In the second subproblem, kinetic rate constants for chain transfer, reactivation and the formation and propagation of 2,1-inserted chains were estimated from molecular weight data and measurements of butenyl (B) and isobutyl end group (I) percentages by minimizing the following least-squares objective function:

$$\min_{\theta_2} \sum_{i=1}^{N_i} \left(\left[\frac{M_n(t_f^i) - \hat{M}_n(t_f^i)}{M_n(t_f^i)} \right]^2 + \left[\frac{M_w(t_f^i) - \hat{M}_w(t_f^i)}{M_w(t_f^i)} \right]^2 + \left[\frac{B(t_f^i) - \hat{B}(t_f^i)}{B(t_f^i)} \right]^2 + \left[\frac{I(t_f^i) - \hat{I}(t_f^i)}{I(t_f^i)} \right]^2 \right) \tag{21}$$

where t_f^i is the final time for the ith experiment. The kinetic rate constants $\theta_2 = \{k_M, k_H, k_{rH}, k_s, k_{sp}, k_{sM}, k_{Al}, k_{rAl}\}$ served as decision variables, while the first set of kinetic parameters (θ_1) were fixed at their previously estimated values.

The parameters θ_2 had some effect on reaction rate and θ_1 affected both MWD and the percentages of end groups. Therefore, the final step in the optimization procedure was to combine both objective functions 20 and 21 to perform a one-step optimization for all the kinetic parameters. Kinetic parameter values obtained from the previous subproblems were used as the initial guess. Weighting factors were used to scale the absolute value of the two objective functions. The resulting optimization problem was solved by temporally discretizing the kinetic model in eqs 5−19 using orthogonal collocation on finite elements.[50] The mathematical programming language AMPL (AMPL Optimization LLC, Albuquerque, NM) and the nonlinear solver CONOPT (ARKI Consulting & Development A/S, Bagsvaerd, Denmark) were used to minimize the objective functions with the kinetic model equations posed as equality constraints.[51]

Acknowledgment. We thank Dr. Luigi Resconi for kindly donating the metallocene catalyst *rac*-Et(4,7-Me_2-1-Ind)$_2ZrCl_2$. We also thank Albemarle Corp. for donating the MAO solution. Funding for this work was provided in part by the General Electric Corporation and the University of Massachusetts. Central analytical facilities used in these studies were supported by the NSF-sponsored Materials Research Science and Engineering Center on Polymers at UMass Amherst (DMR-0213695).

References and Notes

(1) Spaleck, W.; Kuber, F.; Winter, A.; Rohrmann, J.; Bachmann, B.; Antberg, M.; Dolle, V.; Paulus, E. F. *Organometallics* **1994**, *13*, 954−963.
(2) Kaminsky, W. *J. Chem. Soc., Dalton Trans.* **1998**, 1413−1418.
(3) Coates, G. W. *Chem. Rev.* **2000**, *100*, 1223−1252.
(4) Resconi, L.; Cavallo, L.; Fait, A.; Piamontesi, F. *Chem. Rev.* **2000**, *100*, 1253−1345.
(5) Busico, V.; Cipullo, R. *Prog. Polym. Sci.* **2001**, *26*, 443−533.
(6) Vela-Estrada, J. M.; Hamielec, A. E. *Polymer* **1994**, *35*, 808−818.
(7) Huang, J.; Rempel, G. L. *Ind. Eng. Chem. Res.* **1997**, *36*, 1151−1157.
(8) Thorshaug, K.; Stovneng, J. A.; Rytter, E.; Ystenes, M. *Macromolecules* **1998**, *31*, 7149−7165.
(9) Wester, T. L.; Johnsen, H.; Kittilsen, P.; Rytter, E. *Macromol. Chem. Phys.* **1998**, *199*, 1989−2004.
(10) Ochoteco, E.; Vecino, M.; Montes, M.; De la Cal, J. C. *Chem. Eng. Sci.* **2001**, *56*, 4169−4179.
(11) Nele, M.; Mohammed, M.; Xin, S.; Collins, S. *Macromolecules* **2001**, *34*, 3830−3841.
(12) Kaminsky, W.; Kulper, K.; Brintzinger, H.-H.; Wild, F. R. W. P. *Angew. Chem., Int. Ed. Engl.* **1985**, *24*, 507−508.
(13) Zurek, E.; Ziegler, T. *Prog. Polym. Sci.* **2004**, *29*, 107−148.
(14) Chien, J. C. W.; Sugimoto, R. *J. Polym. Sci., Part A: Polym. Chem.* **1991**, *29*, 459−470.
(15) Resconi, L.; Fait, A.; Piemontesi, F.; Colonnesi, M.; Rychlicki, H.; Zeigler, R. *Macromolecules* **1995**, *28*, 6667−6676.
(16) Lieber, S.; Brintzinger, H. H. *Macromolecules* **2000**, *33*, 9192−9199.
(17) Naga, N.; Mizunuma, K. *Polymer* **1998**, *39*, 5059−5067.
(18) Resconi, L.; Piemontesi, F.; Franciscono, G.; Abis, L.; Fiorani, T. *J. Am. Chem. Soc.* **1992**, *114*, 1025−1032.
(19) Fan, G.; Dong, J.-Y. *J. Mol. Catal. A: Chem.* **2005**, *236*, 246−252.
(20) Busico, V.; Cipullo, R. *Macromolecules* **1994**, *27*, 7538−7543.
(21) Kang, K. K.; Shiono, T.; Ikeda, T. *Macromolecules* **1997**, *30*, 1231−1233.
(22) Mogstad, A.-L.; Waymouth, R. M. *Macromolecules* **1994**, *27*, 2313−2315.
(23) Belelli, P. G.; Ferreira, M. L.; Lacunza, M. H.; Damiani, D. E.; Brandolin, A. *Polym. Eng. Sci.* **2001**, *41*, 2082−2094.
(24) Lahelin, M.; Kokko, E.; Lehmus, P.; Pitkanen, P.; Lofgren, B.; Seppala, J. *Macromol. Chem. Phys.* **2003**, *204*, 1323−1337.
(25) Gonzalez-Ruiz, R. A.; Quevedo-Sanchez, B.; Laurence, R. L.; Coughlin, E. B.; Henson, M. A. *AIChE J.* **2006**, *52*, 1824−1835.
(26) Lee, I.-M.; Gauthier, W. J.; Ball, J. M.; Iyengar, B.; Collins, S. *Organometallics* **1992**, *11*, 2115−2122.
(27) Busico, V.; Cipullo, R. *J. Am. Chem. Soc.* **1994**, *116*, 9329−9330.
(28) Liu, Z.; Somsook, E.; Landis, C. R. *J. Am. Chem. Soc.* **2001**, *123*, 2915−2916.
(29) Busico, V.; Cipullo, R.; Esposito, V. *Macromol. Rapid Commun.* **1999**, *20*, 116−121.
(30) Resconi, L.; Piamontesi, F.; Camurati, I.; Balboni, D. *Organometallics* **1996**, *15*, 5046−5059.
(31) Carvill, A.; Zetta, L.; Zannoni, G.; Sacchi, M. C. *Macromolecules* **1998**, *31*, 3783−3789.
(32) Resconi, L.; Camurati, I.; Sudmeijer, O. *Top. Catal.* **1999**, *7*, 145−163.
(33) Quevedo-Sanchez, B.; Henson, M. A.; Coughlin, E. B. *J. Polym. Sci., Part A: Polym. Chem.* **2006**, *44*, 3724−3728.
(34) Resconi, L. *J. Mol. Catal. A: Chem.* **1999**, *146*, 167−178.
(35) Kawahara, N.; Kojoh, S.; Toda, Y.; Mizuno, A.; Kashiwa, N. *Polymer* **2004**, *45*, 355−357.
(36) Kawahara, N.; Kojoh, S.; Matsuo, S.; Kaneko, H.; Matsugi, T.; Toda, Y.; Mizuno, A.; Kashiwa, N. *Polymer* **2004**, *45*, 2883−2888.
(37) Tsutsui, T.; Kashiwa, N.; Mizuno, A. *Makromol. Chem., Rapid Commun.* **1990**, *11*, 565−570.
(38) Resconi, L.; Piamontesi, F.; Camurati, I.; Sudmeijer, O.; Nifant'ev, I. E.; Ivchenko, P. V.; Kuz'mina, L. G. *J. Am. Chem. Soc.* **1998**, *120*, 2308−2321.
(39) Grassi, A.; Zambelli, A. *Macromolecules* **1988**, *21*, 617−622.
(40) Rieger, B.; Mu, X.; Mallin, D. T.; Rausch, M. D.; Chien, J. C. W. *Macromolecules* **1990**, *23*, 3559−3568.
(41) Prosenc, M. H.; Brintzinger, H. H. *Organometallics* **1997**, *16*, 3889−3894.
(42) Hart, J. R.; Rappe, A. K. *J. Am. Chem. Soc.* **1993**, *115*, 6159−6164.
(43) Yoshida, T.; Koga, N.; Morokuma, K. *Organometallics* **1995**, *14*, 4.
(44) Cavallo, L.; Guerra, G. *Macromolecules* **1996**, *29*, 2729−2737.
(45) Liu, J.; Stovneng, J. A.; Rytter, E. *J. Polym. Sci., Part A: Polym. Chem.* **2001**, *39*.
(46) Carvill, A.; Tritto, I.; Locatelli, P.; Sacchi, M. C. *Macromolecules* **1997**, *30*, 7056−7062.
(47) Busico, V.; Cipullo, R.; Cutillo, F.; Vacatello, M. *Macromolecules* **2002**, *35*, 349−354.
(48) Nele, M.; Collins, S. *Macromolecules* **2000**, *33*, 7249−7260.
(49) Nele, M.; Pinto, J. C.; Mohammed, M.; Collins, S. *J. Polym. Sci., Part A: Polym. Chem.* **2005**, *43*, 1797−1810.
(50) Finlayson, B. A. *Nonlinear Analysis in Chemical Engineering*; McGraw-Hill: New York, 1980.
(51) Fourer, R.; Gay, D. M.; Kernighan, B. W. *AMPL: A Modeling Language for Mathematical Programming*, 2nd ed.; Duxbury Press/Brooks/Cole Publishing Company: Boston, MA, 2002.

MA060880N